Acta
Technica
Jaurinensis

Vol. 8, No.3, pp. 201-217, 2015
DOI: 10.14513/actatechjaur.v8.n3.377
Available online at acta.sze.hu

Stress Analysis and Weight Reduction of a One-Cylinder Engine Crankshaft

P. Horváth, J. Égert

**Department of Applied Mechanics, Faculty of Mechanical Engineering
Information Technology and Electrical Engineering
Széchenyi István University
9026 Győr 1 Egyetem tér, Hungary
horvpe@sze.hu, egert@sze.hu**

Abstract: The paper deals with the weight reduction and the achievement of a more homogeneous stress distribution of a one-cylinder engine's crankshaft, developed for the Formula Student series. In order to achieve this goal, a series of static FEM analysis were performed on the crankshaft. For the FEM analyses, the critical loading and kinematic boundary conditions of the crankshaft were calculated with two different methods. The loads were determined analytically and were verified by Creo Mechanism software. The calculations were done for different engine speeds and - as a result - the critical engine speed, where the highest loads appear could be determined. An essential weight reduction and a more homogeneous stress distribution were achieved on the crankshaft as the result of FEM analysis.

Keywords: crankshaft, finite element method (FEM), weight reduction, stress distribution

1. Introduction

The paper shows the stress analysis of the crankshaft of a one-cylinder engine, designed by the SZEngine team (the stundent's engine development team of Széchenyi István University) for the Formula Student (FS) race series and gives recommendations for the weight reduction of the crankshaft. The FS race tracks feature many curves, slaloms and short, straight sections. These features must also be taken into consideration in the course of designing and developing the proper engine for the race car. The main objective of the engine design is the creation of an engine with the possible lowest weight and the possible highest performance. In order to be able to reduce the weight of the crankshaft, a series of static FEM analysis were performed on the crankshaft. On the basis of the results gained by the analysis, one could reduce the weight of the crankshaft, make the stress distribution more homogenous, and fix the emerging failures in the construction. For the analysis, it is necessary to exactly know the maximum loads acting on the crankshaft therefore – as the first step – the paper deals with this problem. The second part shows the results of the stress analyses and the weight reduction.

The analyzed crankshaft (Fig. 1.) is a construction made of three parts, consisting of a crankpin and two other parts, which includes a web, a counterweight and a half-shaft. The three parts are assembled by an interference fit. The material of the crankshaft is 42CrMo4 alloy steel, while for balancing the crankshaft, tungsten hard metal rods are used, which are also connected by an interference fit into the bores of the counterweight. The material properties of the crankshaft are summarized in *Table 1.*

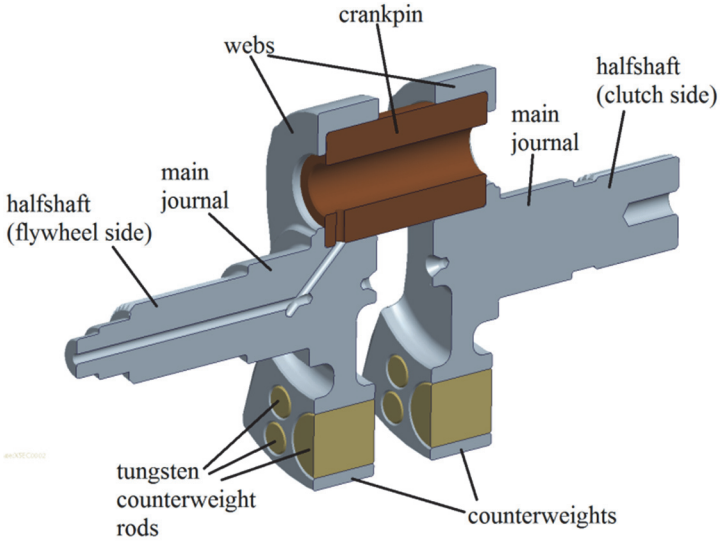

Figure 1. The parts of the analyzed crankshaft

Table 1. Material properties of the crankshaft

Material property	42CrMo4 steel	Tungsten	Unit
Density	7850	19250	kg/m^3
Young's modulus	210000	411000	MPa
Poisson's ratio	0,3	0,28	-
Yield stress	750	1510	MPa
Coefficient of thermal expansion	$1{,}2 \cdot 10^{-5}$	$4{,}3 \cdot 10^{-6}$	1/°C

2. Critical working loads of the crankshaft

The first task is to determine the loads acting on the crankshaft [1], [12], to specify each kind of loading in function of the crank angle and the engine speed. From the loading function the critical maximum loads have to be determined – at which the FEM analysis must be performed.

2.1 Assortment of the working loads

The loads acting on the crankshaft can basically be divided into two groups: loads, which are function of the crank angle and the engine speed, as well as constant loads which are not depending on the revolution. Loads, which are function of the crank angle and the engine speed, originate from three effects:

1) Surface loading acting on the crankpin. These loads originate from the gas pressure inside the engine's cylinder and from the forces of inertia occurring due to the acceleration of the connecting rod and the piston.
2) Body forces resulting from the revolution of the crankshaft.
3) Torque of the flywheel acting on the crankshaft, which occurs due to the moments of inertia of the flywheel and the speed-irregularity (angular acceleration) of the crankshaft.

The constant loads are coming from two effects:

1) Loads from the interference fits (overlap joints).
2) Loads coming from the thermal effects in the engine.

2.2 The surface loads acting on the crankpin

The surface loading acting on the crankpin can basically be determined by two methods: either by using a kind of commercial software dealing with dynamic analysis (for example ADAMS or Creo Mechanism) or by analytically using the principle of impulse and the principle of angular momentum [2]. We determined these loads analytically, but the module of the Creo Mechanism [10], [11] was also used for the verification of the analytically calculated loading.

The gas pressure characteristics were determined by the SZEngine team and it was available in the operating range of the engine (4000-12000 rpm) in 500 rpm angular velocity steps.

During analytical calculations, the angular velocity of the crankshaft was presumed constant, which largely simplifies the calculations, while the failure rate remains at a small value, below 1 % according to [5]. In the course of calculations, at first the kinematic and then the dynamic feature of the connecting rod were determined. After this, the force acting on the crankpin will be derived already from the Newton's law of action and reaction. The kinematic characteristics of the connecting rod were determined on the basis of [3] except for (8) and (11).

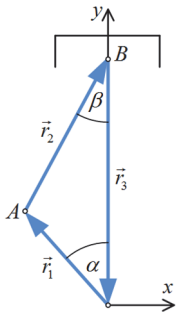

Figure 2. Vector-model of the crank mechanism

In Fig. 2. the vector $\vec{r}_2$ represents the connecting rod and $\vec{r}_1$ models the crank. On the basis of Fig. 2., the following vector-equation can be written:

$$\vec{r}_1 + \vec{r}_2 + \vec{r}_3 = \vec{0}\,. \tag{1}$$

Differentiating once the above vector-equation with respect to time, we get the angular velocity of the connecting rod, while differentiating it twice, the angular acceleration of the connecting rod can be achieved.

$$\omega_2 = \frac{-\omega_1 r_1 \cos\alpha}{r_2 \cos\beta}, \tag{2}$$

$$\varepsilon_2 = \frac{\omega_1^2 r_1 \sin\alpha + \omega_2^2 r_2 \sin\beta}{r_2 \cos\beta}\,. \tag{3}$$

The acceleration of point A is known therefore the acceleration of the arbitrary point P of the connecting rod can be determined by using the angular velocity and the angular acceleration:

$$\vec{a}_P = \vec{a}_A + \vec{\varepsilon}_2 \times \vec{r}_{AP} - \omega_2^2 \vec{r}_{AP}\,, \tag{4}$$

From the evaluation of each term (4), the acceleration of an arbitrary point P is:

$$\begin{aligned}\vec{a}_P = {} & (r_1\omega_1^2 \sin\alpha - \varepsilon_2 r_{AP} \cos\beta + \omega_2^2 r_{AP} \sin\beta)\vec{e}_x + \\ & + (-r_1\omega_1^2 \cos\alpha - \varepsilon_2 r_{AP} \sin\beta - \omega_2^2 r_{AP} \cos\beta)\vec{e}_y\end{aligned} \tag{5}$$

Knowing the mass properties m_h, J_h of the connecting rod and the mass m_d of the piston and the acceleration of an arbitrary point P specified above, the forces acting on the connecting rod (Fig. 3.) can be determined. In Fig. 3. the notation S means the center of gravity of the connecting rod.

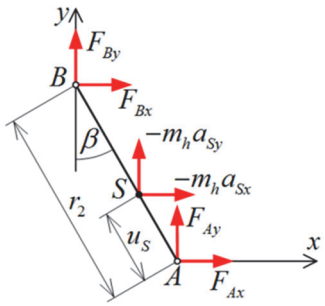

Figure 3. Forces acting on the connecting rod

Applying the principle of impulse for the piston in y direction:

$$m_d a_d = F_g + (-F_{By}) \quad \Rightarrow \quad F_{By} = F_g - m_d a_d\,. \tag{6}$$

Applying the principle of impulse for the connecting rod in y direction:

$$F_{By} + F_{Ay} = m_h a_{Sy} \quad \Rightarrow \quad F_{Ay} = m_h a_{Sy} - F_{By} \,. \tag{7}$$

Applying the principle of angular momentum for the connecting rod rotating about the point *B*:

$$\underline{\underline{J}}_S \vec{\varepsilon}_2 + \vec{\omega}_2 \times \left(\underline{\underline{J}}_S \vec{\omega}_2 \right) + \vec{r}_{BS} \times m_h \vec{a}_S + m_h \left(\vec{\omega}_2 \times \vec{r}_{BS} \right) \times \vec{v}_B = \vec{M}_B \,, \tag{8}$$

where $\vec{v}_B = v_B \vec{e}_y$ is the velocity of point *B,* which value can be determined in the following way:

$$v_B = -\omega_1 r_1 \sin\alpha - \omega_2 r_2 \sin\beta \,. \tag{9}$$

It is important to note that many of the literature sources, such as literature [3] gives only the incomplete form of the principle of angular momentum for a rigid body, which does not contain the fourth term on the left side of the equation (8). According to [6], however, if the principle of angular momentum for a rigid body is applied to a moving point *B* as in the present case – the principle must be completed by the fourth term containing the velocity of the point *B*. In case of leaving this term, the *x* component of the force acting in point *A* shows equation (10), while – taking into consideration this term – it shows equation (11):

$$F_{Ax} = \frac{J_h \varepsilon + m_h a_{Sy} (r_2 - u_S) \sin\beta + m_h a_{Sx} (r_2 - u_S) \cos\beta - F_{Ay} r_2 \cos\beta}{r_2 \sin\beta} \,, \tag{10}$$

$$F_{Ax} = \frac{J_h \varepsilon + m_h a_{Sy} (r_2 - u_S) \sin\beta + m_h a_{Sx} (r_2 - u_S) \cos\beta - F_{Ay} r_2 \cos\beta + m_h \omega_2 r_{BS} \cos\beta v_B}{r_2 \sin\beta} \tag{11}$$

Applying the principle of impulse for the connecting rod in *x* direction:

$$F_{Ax} + F_{Bx} = m_h a_{Sx} \quad \Rightarrow \quad F_{Bx} = m_h a_{Sx} - F_{Ax} \tag{12}$$

Force acting on the crankpin of the crankshaft *C* will be the counter-force of the force acting on point *A* of the connecting rod:

$$F_{Cx} = -F_{Ax} \,, \quad F_{Cy} = -F_{Ay} \,. \tag{13}$$

At 8000 rpm engine speed, the differently calculated tangential and radial components of the force acting on the crankpin, were performed and compared with the results achieved by Creo Mechanism program (Fig. 4. and 5.). In the course of comparison, a proper match could be observed, but – as it can be seen in the figures – a slight deviation could be noticed between the two analytical solutions, which are presented in the tangential force diagram. It is interesting to observe that if the component in *x* direction of force F_A was calculated by applying the incomplete form of the principle of angular momentum (10), an exact match with the result provided by Creo was to be obtained.

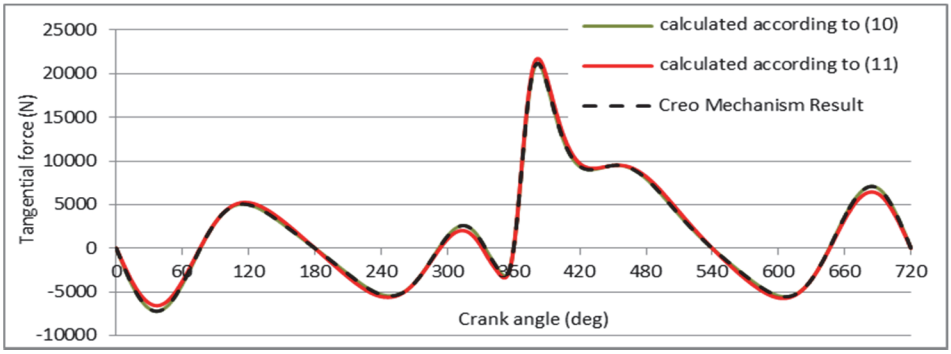

Figure 4. The tangential force acting on the crankpin in function of crank angle at crankshaft speed of 8000 rpm with different calculation methods

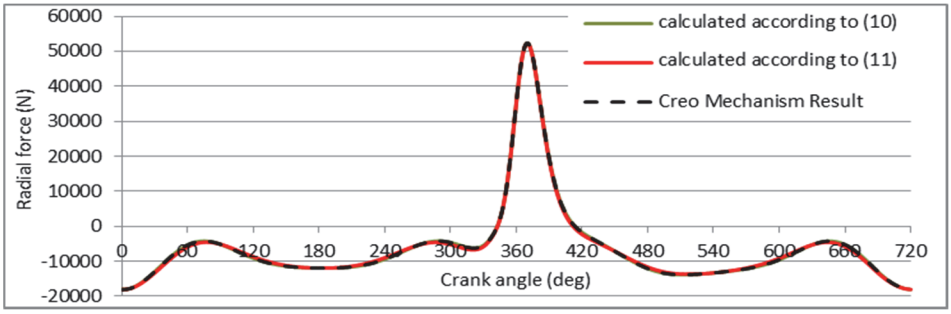

Figure 5. The radial force acting on the crankpin in function of crank angle at crankshaft speed of 8000 rpm with different calculation methods

In reality, the force does not act at a certain point, but on a cylindrical contact surface. The crankpin is assumed to have a sinusoidal pressure distribution. Therefore, the force acting on the crankpin – that was determined above – was transformed into a sinusoidal pressure distribution acting over an angle of $\gamma = 120^{\circ}$ (Fig. 6.).

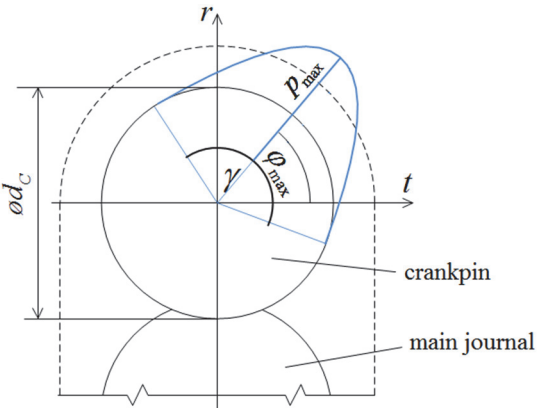

Figure 6. The sinusoidal pressure distribution acting on the crankpin

The pressure curve along the contour of crankpin can be prescribed by the following formula:

$$p(\varphi) = p_{\max} \sin\left[\frac{180}{\gamma}\varphi - \left(\frac{180}{\gamma}\varphi_{\max} - 90\right)\right], \tag{14}$$

where the value $\varphi = 0^{\circ}$ belongs to the *t* axis.

In (14) the pressure constant $p_{\max}$ can be achieved by integrating the pressure surface:

$$F_C = p_{\max} \int_0^{\frac{d_C \pi \gamma}{360}} \int_0^{w_C} \sin\left(\frac{360}{d_C \gamma} s\right) dz\, ds \quad \Rightarrow \quad p_{\max} = \frac{180 F_C}{w_C d_C \gamma}, \tag{15}$$

where w_C is the width and d_C is the diameter of the crankpin.

Since the load acting on the crankpin is the function of the engine speed, with the aid of the equations calculated above, it must be examined in the operational range of the engine (4000 – 12000 rpm) how the loads depend on the change in the engine speeds. At lower engine speeds, the force from gas pressure, while at higher engine speeds, the forces of inertia will be significant. The forces of inertia increase quadratic with the increase of the engine speed. Fig. 7. illustrates the variation of the loads acting on the crankpin at both ends of the operating range.

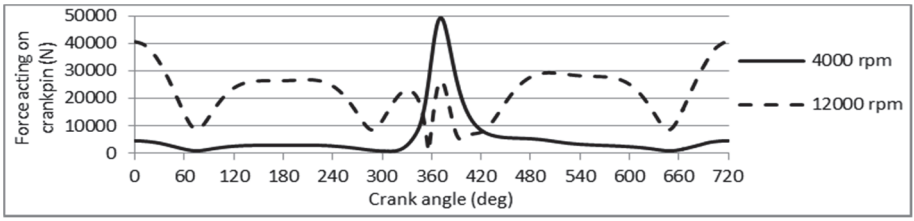

Figure 7. The loads acting on the crankpin in the function of crank-angle at both ends of the operational range

The FEM analysis should be performed at the engine speed, at which the load acting on the crankpin has the maximum value. Fig. 8. shows that the maximum occurs at 6500 rpm engine speed.

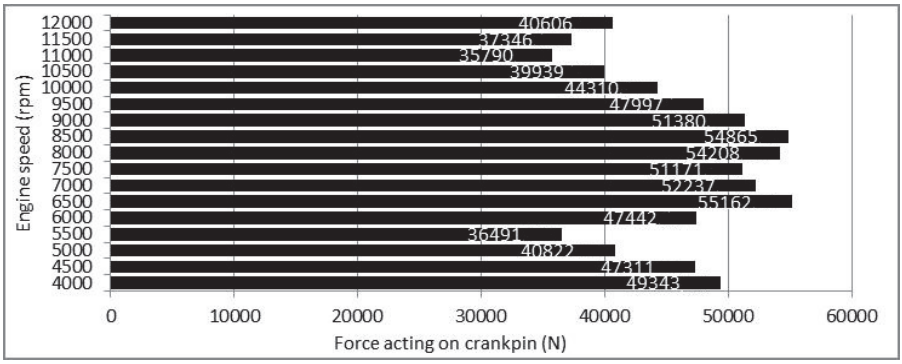

Figure 8. The maximum values of the resultant forces acting on the crankpin in the function of engine speed

2.3. The forces of inertia resulting from the speed irregularity of the crankshaft

This section discusses the instantaneous angular acceleration, which is necessary for the calculation of the body forces resulting from the rotation of the crankshaft, as well as for calculating the torque originating from the flywheel.

The tangential force acting on the crankpin is continuously changing in the function of the crank angle, as it can be seen in Fig. 4. Since the torque of the engine is provided by this force, the torque of the engine will also be irregular, so it will depend on the crank angle.

The inertia of the crankshaft is increased by the flywheel mounted at the end of the crankshaft, which also serves as an energy storing unit. When the instantaneous torque is higher than the medium torque, the crankshaft accelerates, while the flywheel picks up energy. When the instantaneous torque is lower than the medium torque, the crankshaft slows down, while the flywheel delivers energy back to the crankshaft. In the majority of engines, the flywheel – which also includes the clutch – is mounted on one side of the crankshaft. In case of the analyzed single-cylinder engine, the clutch and the flywheel are mounted as two separate parts at both ends of the crankshaft.

In order to be able to determine the speed irregularity, as a first step the medium torque must be calculated. This is a torque value supposed to be constant, which performs the same amount of work as the varying (actual) torque. For this, the torque curve must be integrated for a whole engine cycle and the height of a rectangle of the same width provides the medium value on the basis of the equality of the surfaces.

Fig. 9. illustrates the instantaneous torque and the medium torque at crankshaft speed of 6500 rpm. The work below the medium torque – marked by red stripes – is negative and this decreases the angular velocity, while the work above the medium torque – marked by green stripes – is positive thus increasing the angular velocity.

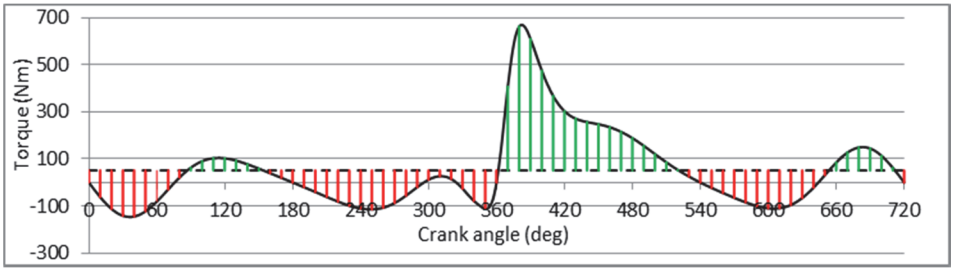

Figure 9. Instantaneous and medium torque acting on the crankshaft at crankshaft speed of 6500 rpm

The instantaneous angular velocity can be obtained from the instantaneous total energy of the system (crankshaft, clutch and flywheel). At first the total energy of the system at $t = 0$ must be determined and then the negative and positive work marked with red and green stripes in Fig. 9. must be added to this average value. So, the total energy of the system at a given time and crank-angle is:

$$E(\alpha_n) = E_0 + \int_0^{\alpha_n} \left[M(\alpha) - M_K \right] d\alpha \,, \tag{16}$$

where E is the energy, resulting from the rotation of the crankshaft, clutch and flywheel and M_K is the medium torque. Knowing the instantaneous total energy of the system, the instantaneous angular velocity of the crankshaft can easily be determined:

$$\omega_1(\alpha) = \sqrt{\frac{2E(\alpha)}{J_f + J_t + J_l}} \,. \tag{17}$$

where J_f, J_t, J_l are the moments of inertia with respect to rotation-axis of the crankshaft, the clutch and the flywheel.

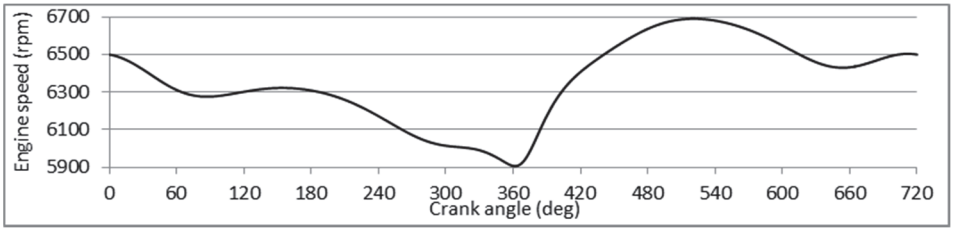

Figure 10. Variation of crankshaft speed at initial crankshaft speed of 6500 rpm

The flywheel – with its high inertia – tends to decrease the irregularity during the work of the engine. This balancing effect causes high torque on the crankshaft. The torque, resulting from the inertia of the flywheel can be calculated by multiplying the inertia of the flywheel with the instantaneous angular acceleration, which is the derivative of the instantaneous angular velocity with respect to time:

$$\vec{M}_t = -J_l \vec{\varepsilon}_l = -J_l \frac{d\vec{\omega}_l}{dt} \,. \tag{18}$$

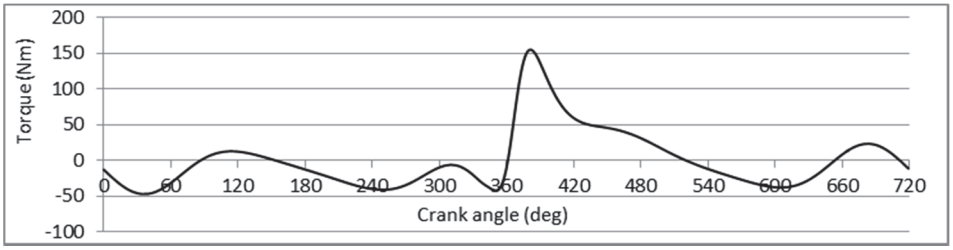

Figure 11. Variation of torque caused by the flywheel at crankshaft speed of 6500 rpm

2.4. Constant loads

In the crankshaft the crankpin is mounted by interference fit and the tungsten rods applied as counterweights are also fit by interference. At these fits / joints – due to the applied interferences – constant loads occur. The interferences were available as constructional parameters. Due to the lack of thermal analysis of the engine, 100 °C

constant, homogenous temperature distribution was supposed as thermal loading on the whole volume of the crankshaft.

3. FEM analysis of the crankshaft

In order to be able to reduce the weight of the crankshaft and to make the stress distribution on it more homogenous, a series of static FEM analysis [7], [8], [9] were conducted on the crankshaft.

3.1. Creating the mechanical and FEM model

The FEM-mesh was created by ANSYS Workbench software [4]. The crankshaft was meshed in quadratic tetrahedron elements. The generally applied element size was 3 mm, while in areas considered to be critical (like the main journal fillet or surfaces connected by interference fit), element sizes of 1 and 2 mm were applied. The total number of elements is 188 152 which contain 306 788 nodes. In the previous chapter it has been stated that the crankshaft receives the highest loading at 6500 rpm engine speed, therefore the finite element analysis was carried out at this nominal engine speed. Fig. 12. shows the meshed crankshaft, while the areas of boundary conditions and applied loads are illustrated in Fig. 13.

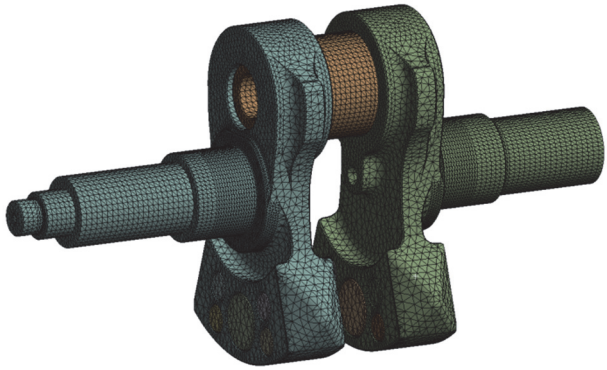

Figure 12. FEM model of the crankshaft

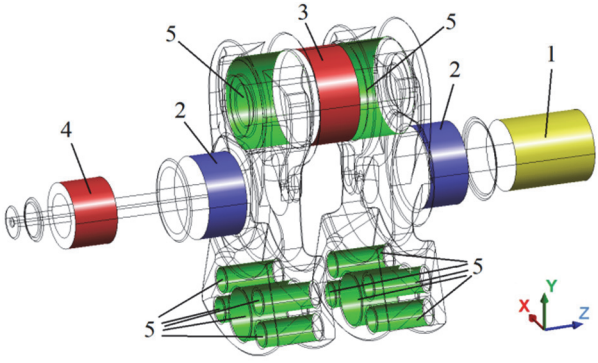

1. Clutch contact surface fixed in rot-z direction
2. Elastic support on the contact surface of the main journals bearings
3. Sinusoidal pressure distribution
4. Torque applied on the contact surface of the flywheel
5. loads resulting from interference

Other loads:

- body forces caused by angular velocity
- 100 °C heat load

Figure 13. The areas of boundary conditions and applied loads

3.2. Evaluation of the finite element analysis

In the course of the finite element analysis, the stress distribution of each special load was examined at first separately thereby the weight of each load could be determined. Then the stress distribution of the total load was also calculated, on the basis of which the possible weight reduction may be performed.

3.2.1. Stress distributions from constant loads

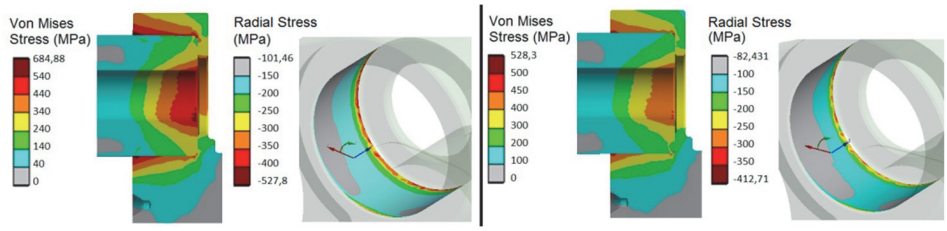

(a) Interference of 0,1 mm *(b) Interference of 0,08 mm*

Figure 14. Von Mises stress distribution and the radial stress distribution on the surface of the bore of the crank-throw

Fig. 14. illustrates the von Mises stress distribution and the radial stress distribution (negative contact pressure distribution) occurring on the surface of the bore of the webs occurring as a result of interference of 0,1 and 0,08 mm, i.e. at both ends of the tolerance range. From this figure, it can be stated that – in both cases – very high von Mises stresses occur furthermore the maximum values of the contact pressure ensuring the joint are also rather high presumably the application of smaller interference would be sufficient. As a result of the 0,01 mm interference of the hard metal rod which serves as counterweight, on the counterweight part, about 300 MPa maximum von Mises stresses occurred.

During the analysis of the thermal load, the above mentioned kinematic boundary conditions were not applied, since – as a result of the thermal effects – the parts ensuring the kinematic boundary conditions would also expand and this could not have been taken into account by the modeling. As a result of the thermal load, not too high stresses occurred. The equivalent von Mises stresses of about 300 MPa occurring at interference fit of the counterweights decreased by half due to the different coefficients of thermal expansion of tungsten and steel (Fig. 15.).

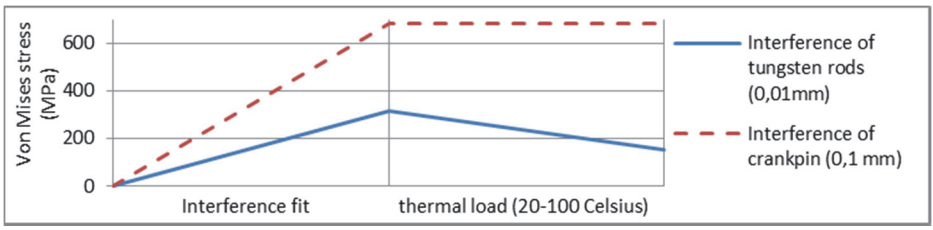

Figure 15. Maximum von Mises stresses occurring as a result of interference fits and the thermal load

3.2.2. Stress distributions from varying loads in function of crank angle

Fig. 16. illustrates the maximum von Mises stresses caused by the varying loads in function of crank angle.

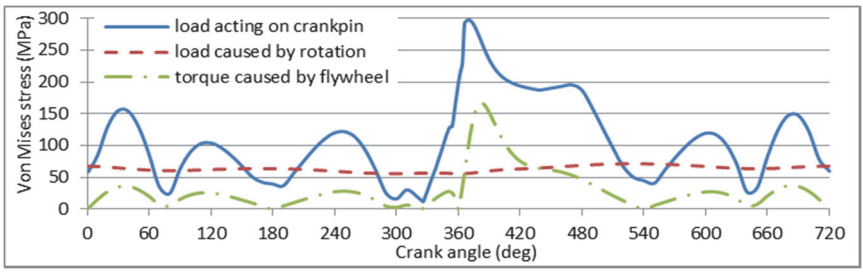

Figure 16. Variation of maximum von Mises stresses caused by the individual loads in function of crank angle

Fig. 17. shows the stress distribution of each load at the crank angle, where the maximum von Mises stress occur. On the basis of the results, the following conclusions could be drawn:

- The maximum equivalent von Mises stress acting on the crankpin occurs at 371^{o} crank angle, this means around the ignition its magnitude is about 300 MPa. The maximum von Mises stresses occur between the fillet of the web and at the main journal (Fig. 17.a).
- The maximum von Mises stress caused by the forces of inertia varies according to the angular velocity. The stresses occurring here are much lower compared to stresses caused by former two loads (max. 70 MPa). The highest stresses are occurring between the main journal and the counterweight (Fig. 17.b).
- The maximum von Mises stress occurring as a result of the torque caused by the flywheel varies according to the variation of the torque. The highest stresses occur on the surface of the half shafts (Fig. 17.c).

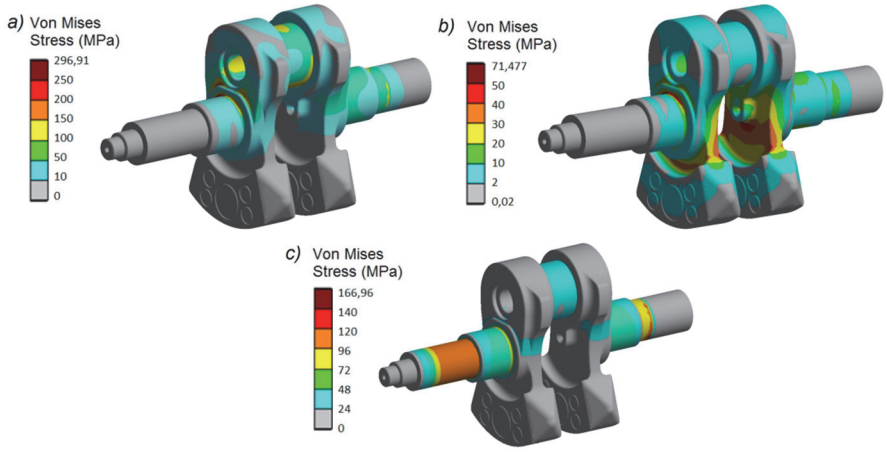

Figure 17. The maximum von Mises stresses occurring from
a) loads on the crankpin b) rotation of the crankshaft c) torque by the flywheel

3.2.3. Checking the effect of the element's size

In order to check the accuracy of the applied finite element-mesh discussed in chapter 3.1, the above described analysis was carried out with two different element size-variations as well, including a denser / finer mesh - the size (number of elements) of which was double of the original mesh - as well as a coarser mesh, the size of which was half of the original mesh.

Fig. 18.*a* illustrates the maximum Von Mises stresses in case of different loads and different element sizes. Fig. 18.b illustrates the minimum radial stresses (maximum contact pressure) on the surface of the web's hole in case of 0,1 mm interference. As it can be seen from the figures, in general, the difference between the original and the finer mesh is smaller than the difference between the original and the coarser mesh, so the values converge by fining the mesh. In case of interference fit, practically there is no difference between the results provided by the original and by the finer mesh. There is no essential difference between the results of the original and those of the finer mesh in other cases, either. Considering this small difference and the significantly higher computation resources demanded by a finer mesh, the further analysis was performed with the original mesh.

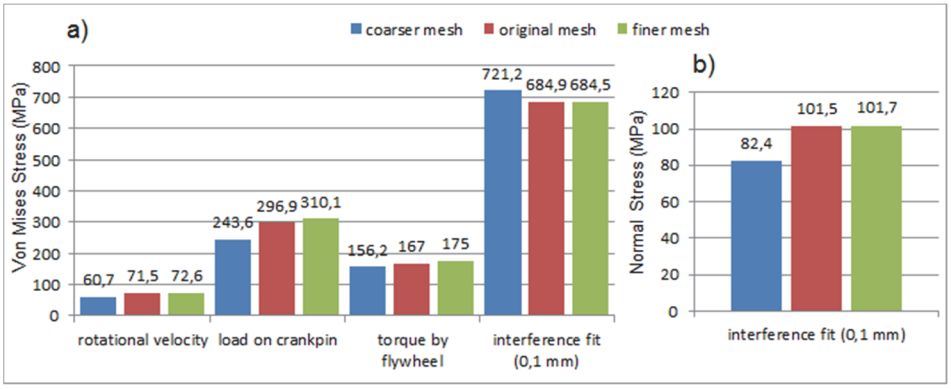

Figure 18. The maximum von Mises and radial stresses in case of different loads and different mesh density

3.2.4. Stress distributions from total load

Fig. 19. demonstrates the stress distributions caused by critical total load.

At the critical total load, the following statements can be made:

- The highest von Mises stresses occurred from the interference fit between the web and the crankpin. This interference loading causes the dominant influence on the stress distribution.

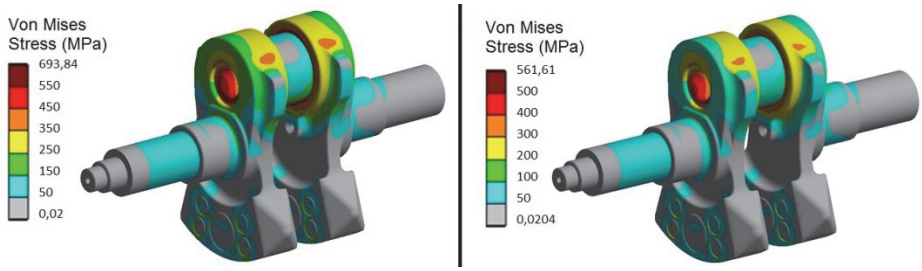

(a) Interference of 0,1 mm *(b) Interference of 0,08 mm*

Figure 19. Equivalent von Mises stress distributions caused by critical total load

- The maximum stress values do not depend on the angle position, so the variation of the stress caused by total load will be approximately constant in function of crank angle.
- The fact that stresses caused by interference are dominating, can be regarded as a constructional failure. Therefore – prior to the weight reduction – this constructional failure should be fixed.

3.2.5. Correction of the constructional failure

On the basis of the aforementioned, stress caused by interference is too high furthermore the contact pressure ensuring the contact is also more than necessary. Therefore this constructional failure had to be eliminated first. In order to be able to determine the minimum necessary contact pressure, it has to be examined how the minimum value of the contact pressure varies on the surface of the bore of the web while applying the total load during a whole engine cycle.

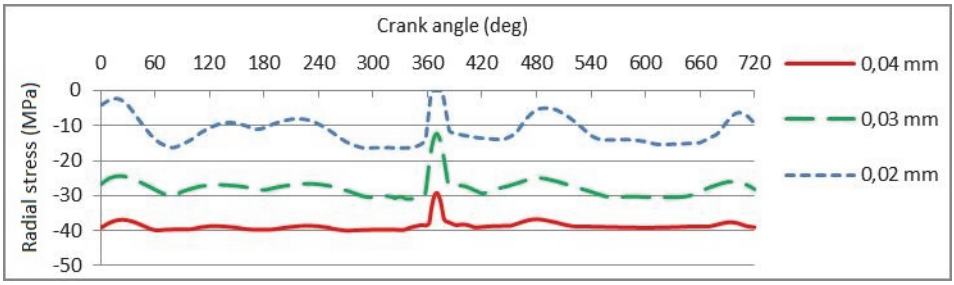

Figure 20. Variation of the minimum radial stress (maximum contact pressure) in function of crank angle in case of different interferences

In case of interference of 0,02 mm, the minimum value of the contact pressure around ignition reaches zero value, so there will be disconnection between the crankpin and the bore, it is to be feared that the crankpin will become loose, therefore at least 0,03 mm interference is necessary in order to be able to properly ensure the interference fit (Fig. 20.). As there is no torsional or axial load between the crankpin and the bore of the web, sliding won't occur between connecting components, so we didn't take it into consideration.

3.3. The modified geometry

On the basis of the results of the finite element analysis, it can be stated that the stress distribution of the crankshaft is not too homogenous. There are areas in which only very small stresses occur, so it is reasonable to remove material from there, while in other areas too high stresses occur, so they must be reduced by proper constructional modifications. The modifications that were carried out can be summarized as follows:

- Increase of the inner bore's diameter of the shafts and pins: higher stresses typically occur on the outer surface of the shafts / pins, while only minimum stresses occur inside them, therefore it is reasonable to remove material from there. In case of the inner bores, the following modifications were carried out:
  - The diameter of the oil bore was increased from 3 mm to 10 mm
  - The diameter of the bore on the clutch side was increased from 8 mm to 16 mm, while its depth was increased from 20 mm to 64,5 mm
  - The inner bore of the crankpin was increased from 15 mm to 20 mm
- The following modifications were carried out in the geometry of the webs:
  - Removal of the "ears" of the webs. Since only small stresses occurred here, they have been removed in order to reduce the weight.
  - Removal of the "shoulder part" of the webs, as a result of which weight reduction was achieved on the one hand, while on the other hand, the stress distribution resulting from the interference fit between the web and the crankpin could be made more homogenous.
  - Reduction of the width and thickness of the web in order to be able to reduce the weight.
  - The rounding / fillet between the main journal and the web was increased from 1,5 mm to 2 mm, by which – as a result of the load acting on the crankpin – the highest stress occurring at the fillet area could be reduced and therefore the stress distribution could be made more homogenous.
- Modification of the counterweight part. Due to the modifications carried out in the previous two steps, the balance of the crankshaft has changed. Due to the increase of the inner bore of the crankpin, as well as due to the removal of material from the upper part of the web, the center of gravity of the crankshaft was shifted into the direction of the counterweights. In order to be able to restore the balance of the crankshaft, the mass of the counterweight had to be reduced. This could be achieved by two kinds of modification:
  - The width and thickness of the counterweight part were reduced.
  - Instead of four small and one large tungsten rods serving as counterweights, five small tungsten rods were installed.

The comparison of the original and modified crankshafts can be seen in Fig. 21.

The extent of the minimum necessary interference was examined by applying the method indicated in chapter 3.2.5. also for case of the modified geometry. In the course of this, it was found that in case of the modified geometry minimum 0,04 mm interference is necessary. Fig. 22. demonstrates the von Mises stress distributions caused by critical total load in the modified construction.

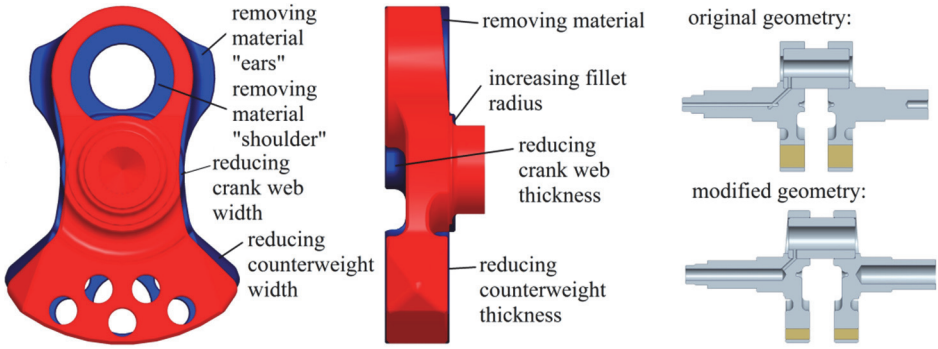

Figure 21. Constructional modifications carried out on the crankshaft

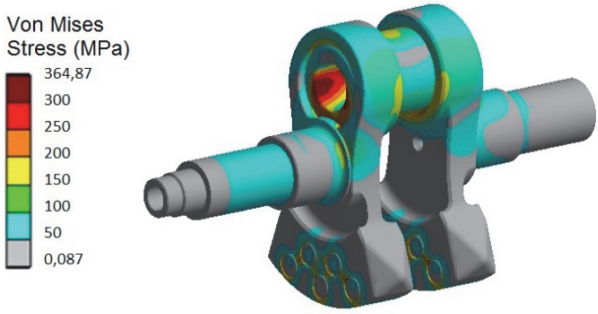

Figure 22: Von Mises stress distribution of the modified crankshaft caused by critical total load

Summary

For the analysis, the critical loads acting on the crankshaft were analytically determined. In the course of this, we have stated that the highest load occurs on the crankshaft at a speed of 6500 rpm, therefore the series of static FEM analysis were performed at this engine speed. The results of the FEM analysis have shown that the crankshaft has a constructional failure, because the equivalent von Mises stress caused by the interference between the crankpin and the web was significantly higher than the stresses caused by the combustion. As a first step, this failure was eliminated by decreasing the extent of the interference. From the FEM analysis it can also be concluded, that there are several areas on the crankshaft, at which very small stresses occur, so material was removed from these areas. As a result of the constructional modifications, the stress distribution became more homogenous furthermore the weight of the crankshaft could be reduced by 19 %.

References

[1] Dezsényi Gy: Design and testing of internal combustion engines (in Hungarian). Nemzeti Tankönyvkiadó, Budapest, 1989.

[2] Montazersadgh FH, Fatemi A: Stress Analysis and Optimization of Crankshafts Subject to Dynamic Loading. International Journal of Materials and Manufacturing, SAE International, Vol. 1, Issue 1, pp. 211-217, April 2009.

[3] Wilson CE, Sadler PJ: Kinematics and Dynamics of Machinery. Harper Collins College Publishers, 1993.

[4] ANSYS 14.5 Mechanical APDL Theory Reference. Ansys Inc., 2012.

[5] Shenoy PS: Dynamic Load Analysis and Optimization of Connecting Rod. Master of Science Degree in Mechanical Engineering, The University of Toledo, 2004.

[6] Király B: Dynamics (in Hungarian). Miskolci Egyetemi Kiadó, Miskolc, 1998.

[7] Zienkiewicz OC, Taylor RL: The Finite Element Method. Fifth edition, Vol. 1. The Basis, Butterworth-Heinemann, 2000.

[8] Zienkiewicz OC, Taylor RL: The Finite Element Method. Fifth edition, Vol. 2, Solid Mechanics, Butterworth-Heinemann, 2000.

[9] Bathe KJ: Finite-Elemente-Methoden. Springer Berlin, 2002.

[10] Toggod R, Zecher J: Creo Parametric 2.0 Tutorial. SDC Publications, 2013.

[11] Chang K-H: Mechanism Design with Creo Elements/Pro 5.0, SDC Publications, 2011.

[12] Pulkrabek WW: Engineering Fundamentals of the Internal Combustion Engine. 2nd Edition, Prentice Hall, 2003.